ISME

The Iranian Journal of Mechanical Engineering Transactions of ISME
Journal homepage: https://jmee.isme.ir/
Vol. 25, No. 2, 2024, pp. 6-25

Research Paper

DOI: https://doi.org/10.30506/jmee.2023.1998743.1314

Hossein Eliasi*
Ph.D. Candidate

Gholamhasan Payganeh†
Associate Professor

Majid Shahgholi‡
Associate Professor

Mohammad Reza Eslami§
Professor

Nonlinear Coupled Thermoelasticity of Cylindrical Shells Resting on Elastic Foundation

Kinematically nonlinear coupled thermoelasticity of the FGM cylindrical shell resting on elastic foundations is investigated under heat shock. The energy and equations of motion are solved simultaneously as a system of equations for an FG cylindrical shell. It is assumed that the shell is resting on the nonlinear Winkler elastic foundation. The classical theory of coupled thermoelasticity along with the first order shear deformation shell theory are used to solve the problem. The finite element method is employed to numerically solve the problem in the space domain and the Newmark method in time domain. Temperature distribution across the shell thickness is considered to be linear. The radial displacement distributions for different values of the power law index and the Winkler coefficients are plotted in terms of time.

Keywords: Nonlinear coupled thermoelasticity, Cylindrical shell, Functionally graded materials, Elastic foundation

1 Introduction

This paper presents an investigation on coupled thermoelasticity of functionallygraded cylindrical shell resting on elastic foundation. Shell structures under thermal shock loads are frequently encountered in the structural design problems. Free vibrations of a cylindrical shell partially resting on elastic foundation is reported in [1]. Paliwal[2] presented the free vibrations of a cylindrical shell on an elastic foundation. These articles deal with the effect of elastic foundation on the vibration behavior of the cylindrical shells.

*Ph.D. Candidate, Department of Mechanical Engineering, Shahid Rajaee Teacher Training University, Tehran, Iran, h.elyasi.m@gmail.com
†Corresponding author, Associate Professor, Department of Mechanical Engineering, Shahid Rajaee Teacher Training University, Tehran, Iran, g.payganeh@sru.ac.ir
‡Associate Professor, Department of Mechanical Engineering, Shahid Rajaee Teacher Training University, Tehran, Iran, majid.shahgholi@sru.ac.ir
§Professor, Department of Mechanical Engineering, Amirkabir University of Technology, Tehran, Iran, eslami@aut.ac.ir

Received: 2023/03/19, Revised: 2023/05/11, Accepted: 2023/09/23

Sofiev[3] presented large amplitude vibrations of FGM orthotropic cylindrical shells interacting with the nonlinear Winkler elastic foundation. The study intends to investigate the large amplitude vibration of functionally graded material cylindrical shells interacting with the nonlinear Winkler elastic foundation in the framework of Donnell's shell theory.
For extremely small thermal shock load periods, the coupled thermoelasticity theory is recommended to be considered [4]. Coupled thermoelasticity of cylindrical shells made of homogeneous, functionally graded materials, and composite materials based on the classical coupled thermoelasticity theory are reported in [5-10]. Coupled thermoelasticity of circular plates made of functionally graded materials under lateral thermal shock load is reported by Jafarinezhad and Eslami [11].
The generalized thermoelasticity of orthotropic cylindrical shells using the perturbation method is reported by Wu et al [12]. Eliasi and Eslami presented coupled thermoelasticity of FGM truncated conical shells [13]. Free vibration analysis of FGM cylindrical shells surrounded by Pasternak elastic foundation in thermal environment, considering fluid-structure interaction, is reported in [14]. Alibeigloo [15] has studied the coupled thermoelasticity of carbon nano tube reinforced composite rectangular plate under thermal shock load.
The present article deals with the nonlinear classical thermoelasticity problem of a Titanium–-Zirconia functionally graded thin cylindrical shell resting on elastic foundation under impulsive thermal shock load, where the kinematical relations are assumed to be nonlinear. The material properties are graded across the thickness direction according to a volume fraction power law distribution. The governing equations are based on the Sanders theory for nonlinear strain-displacement relations. The Galerkin finite element method is used to solve the nonlinear governing equations. The Newmark method for the nonlinear equations is used to obtain the solution in time domain. The solution is verified with the known data in literature for the linear coupled thermoelasticity of thin cylindrical shells and nonlinear coupled thermoelasticity of thin cylindrical shell. The effect of elastic foundation on lateral displacement of cylindrical shell is investigated in this article. The numerical results are obtained for the lateral displacement component under several types of thermal shocks and several power law indices.

2 Analysis

The material properties of the functionally graded shell, such as Young's modules $E(z)$, thermal expansion coefficient $\alpha(z)$, thermal conduction coefficient $k(z)$, specific heat conduction $c(z)$, and density $\rho(z)$ are described across the shell thickness using the power law distribution, where z is the thickness coordinate $\left(-\frac{h}{2} \le z \le \frac{h}{2}\right)$, and h is thickness of the shell. We assume that the functionally graded shell is made of metal-phase and ceramic-phase. It is assume that V_m and V_c represent the volumes of metal and ceramic phases, respectively, and the volume fraction of each constituent material is denoted by

$$f_m = \frac{V_m}{V_m + V_c} f_c = \frac{V_c}{V_m + V_c} \tag{1}$$

$$f_m + f_c = 1 \tag{2}$$

The volume fraction is assumed to follow a power law function as

$$f_m = \left(\frac{2z + h}{2h}\right)^i, \qquad f_c = 1 - f_m \qquad i \ge 0 \tag{3}$$

where i represents the power law index and its variation represents the material variation through the shell thickness. When value of i equals to zero, it represents a fully metal and when infinity it represents a fully ceramic shell. It is assumed that Poisson's ratio is constant across the shell thickness due to its small variations for the constituent materials.

$$\begin{aligned} E(z) &= E_c + E_{mc} f_m \\ \alpha(z) &= \alpha_c + \alpha_{mc} f_m \\ K(z) &= k_c + k_{mc} f_m \\ \rho(z) &= \rho_c + \rho_{mc} f_m \\ c(z) &= c_c + c_{mc} f_m \end{aligned} \tag{4}$$

where

$$\begin{aligned} E_{mc} &= E_m - E_c \\ \alpha_{mc} &= \alpha_m - \alpha_c \\ K_{mc} &= K_m - K_c \\ \rho_{mc} &= \rho_m - \rho_c \\ c_{mc} &= c_m - c_c \end{aligned} \tag{5}$$

In this article, the FG cylindrical shell resting on the nonlinear Winkler elastic foundation is considered. The reaction–-deflection relation of mechanical model for elastic foundation is assumed to be

$$N_w = L_L w_0 + K_{NL} w_0^3 \tag{6}$$

where N_w is the density of reaction force of the elastic foundation, K_L and K_{NL} are the linear and nonlinear Winkler elastic foundation coefficients, respectively, and w is the displacement components in the z-direction.

2.1 Strain-displacement relations

Consider a thin FGM cylindrical shell with length L, thickness h, and mid-thickness radius R. The cylindrical coordinates (x, θ, z) are considered along the axial, circumferential, and radial directions, respectively, as shown in Fig. (1).

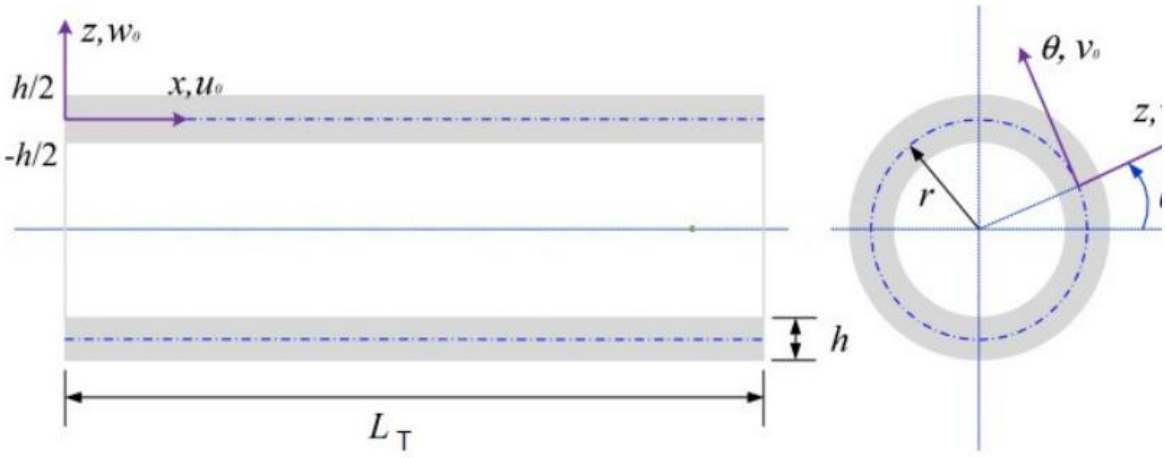

Figure 1 Cylindrical shell resting on elastic foundation with displacement fields

It is assumed that the thermal shock load is axisymmetric. Considering the first-order shear deformation theory, the displacement components in terms of the mid-plane displacements are

$$\begin{aligned} u(x,z,t) &= u_0(x,t) + z\varphi_x(x,t) \\ w(x,z,t) &= w_0(x,t) \end{aligned} \tag{7}$$

Where u_0 and w_0 present the displacement components of the middle surface of the shell and φ_x is the rotation of tangent line to the middle plane about the x-axis.
Normal and shear strains at any point across the thickness of the cylindrical shell at a distance z away from the middle plane according to the nonlinear Sanders assumption are

$$\begin{aligned} \varepsilon_x &= \frac{\partial u_\circ}{\partial x} + z\frac{\partial \varphi_x}{\partial x} + \frac{1}{2}\left(\frac{\partial w_0}{\partial x}\right)^2 \\ \varepsilon_\theta &= \frac{w_0}{r} \\ \gamma_{xz} &= \varphi_x + \frac{\partial w_0}{\partial x} \end{aligned} \tag{8}$$

2.2 Stress-strain relations

According to Hooke's law, the stress-strain relationship is

$$\begin{Bmatrix} \sigma_x \\ \sigma_\theta \\ \tau_{xz} \end{Bmatrix} = \begin{bmatrix} Q_{11} & Q_{12} & 0 \\ Q_{12} & Q_{22} & 0 \\ 0 & 0 & Q_{55} \end{bmatrix} \begin{Bmatrix} \varepsilon_x - \alpha\Delta T \\ \varepsilon_\theta - \alpha\Delta T \\ \gamma_{xz} \end{Bmatrix} \tag{9}$$

where

$$Q_{11} = Q_{22} = \frac{E(z)}{1-\nu^2}, \qquad Q_{12} = \frac{\nu E(z)}{1-\nu^2}, \qquad Q_{55} = \frac{E(z)}{2(1+\nu)} \tag{10}$$

Using Eqs. (8) through (9a) the force and bending moment resultants are

$$\begin{Bmatrix} N_{xx} \\ N_{\theta\theta} \\ M_{xx} \\ M_{\theta\theta} \\ Q_{xz} \end{Bmatrix} = \begin{bmatrix} A_{11} & A_{12} & B_{11} & B_{12} & 0 \\ A_{12} & A_{22} & B_{12} & B_{22} & 0 \\ B_{11} & B_{12} & D_{11} & D_{12} & 0 \\ B_{12} & B_{22} & D_{12} & D_{22} & 0 \\ 0 & 0 & 0 & 0 & A_{55} \end{bmatrix} \begin{Bmatrix} \frac{\partial u_0}{\partial x} + \frac{1}{2}\left(\frac{\partial w_0}{\partial x}\right)^2 \\ \frac{w_0}{R} \\ \frac{\partial \varphi_x}{\partial x} \\ 0 \\ \frac{\partial w_0}{\partial x} + \varphi_x \end{Bmatrix} - \begin{Bmatrix} N^T \\ N^T \\ M^T \\ M^T \\ 0 \end{Bmatrix} \tag{11}$$

where A_{ij}, B_{ij}, and D_{ij} are defined in the Appendix. The thermal force and bending moment resultants are defined as

$$N^T = \int_{-\frac{h}{2}}^{\frac{h}{2}} \frac{E(z)\alpha(z)}{1-\nu^2}\Delta T dz \tag{12}$$

$$M^T = \int_{-\frac{h}{2}}^{\frac{h}{2}} \frac{E(z)\alpha(z)}{1-\nu^2}\Delta T z dz$$

Substituting the strain-displacement and stress-strain relations in the above relations, provides the force and bending moment resultants in terms of the displacement components and temperature for the cylindrical shell.

2.3 Equations of motion and boundary conditions

The Hamilton principle is used to obtain the equations of motion of a thin cylindrical shell resting on elastic foundation. According to Hamilton's principle, the equations of motion are derived through the following variational equation. The kinetic and potential energies and the density of reaction force of the elastic foundation are placed in Hamilton's relation

$$\int_0^t (\delta K - \delta H + \delta W)dt = 0 \tag{13}$$

where K, H, and W are the kinetic energy, strain energy, and the work done by the applied loads of the FG cylindrical shell, including the work done by foundation reaction.
The nonlinear equations of motion of the assumed thin cylindrical shell resting on elastic foundation are then derived as

$$\begin{gathered} N_{xx,x} - I_1\ddot{u}_\circ - I_2\ddot{\varphi}_x = 0 \\ N_{xx,x}(w_{0,x}) - N_{xx}(w_{0,xx}) + \frac{N_{\theta\theta}}{R} - Q_{xz,x} - I_1\ddot{w}_0 - K_L h w_0 - K_{NL} h {w_0}^3 = 0 \\ M_{xx,x} + Q_{xz} - I_2\ddot{u}_\circ - I_3\ddot{\varphi}_x = 0 \end{gathered} \tag{14}$$

where

$$\begin{gathered} I_1 = \int \rho(z)dz \\ I_2 = \int \rho(z)zdz \\ I_3 = \int \rho(z)z^2dz \end{gathered} \tag{15}$$

Using Hamilton's principle, the force and kinematical natural boundaryconditions are derived as

$$\begin{gathered} \mathrm{N}_{xx}(\delta u_0) = \bar{N}_{xx} or u_0 = \bar{u}_0 \\ \mathrm{V}_x(\delta w_0) = \bar{Q}_x + \bar{N}_{xx}\bar{w}_{0,x} or w_0 = \bar{w}_0 \\ M_{xx}(\delta\varphi_x) = \bar{M}_{xx} or \varphi_x = \bar{\varphi}_x \end{gathered} \tag{16}$$

The barred symbols here represent the known values of the parameters. Using the force and bending moment resultants and substituting into the equations of motion, the equations are obtained in terms of the displacement components as

First equation of motion

$$-A_{11}\frac{\partial^2 u_0}{\partial x^2}-A_{11}.\frac{\partial w_0}{\partial x}\frac{\partial^2 w_0}{\partial x^2}-A_{12}\frac{1}{r}\frac{\partial w_0}{\partial x}-B_{11}.\left(\frac{\partial^2 \varphi_x}{\partial x^2}\right)+(R_1+R_{12})\frac{\partial T_0}{\partial x}+(R_2+R_{22})\frac{\partial T_1}{\partial x}-I_1\frac{\partial u_0}{\partial t^2}-I_2\frac{\partial \varphi_x}{\partial t^2}=0 \tag{17}$$

Second equation of motion

$$\begin{aligned}-A_{11}\frac{\partial^2 u_0}{\partial x^2}\left(\frac{\partial w_0}{\partial x}\right)-A_{11}\left(\frac{\partial w_0}{\partial x}\right)^2\left(\frac{\partial^2 w_0}{\partial x^2}\right)-A_{12}\frac{1}{r}\left(\frac{\partial w_0}{\partial x}\right)^2\\ -B_{11}.\left(\frac{\partial^2 \varphi_x}{\partial x^2}\right)\left(\frac{\partial w_0}{\partial x}\right)+(R_1+R_{12})\frac{\partial T_0}{\partial x}\left(\frac{\partial w_0}{\partial x}\right)\\ +(R_2+R_{22})\frac{\partial T_1}{\partial x}\left(\frac{\partial w_0}{\partial x}\right)-A_{11}\frac{\partial u_0}{\partial x}\left(\frac{\partial^2 w_0}{\partial x^2}\right)\\ -A_{11}\frac{1}{2}\left(\frac{\partial w_0}{\partial x}\right)^2\left(\frac{\partial^2 w_0}{\partial x^2}\right)-A_{12}\frac{1}{r}w_0\left(\frac{\partial^2 w_0}{\partial x^2}\right)\\ -B_{11}\left(\frac{\partial^2 w_0}{\partial x^2}\right)\left(\frac{\partial \varphi_x}{\partial x}\right)+(R_1+R_{12})T_0\left(\frac{\partial^2 w_0}{\partial x^2}\right)\\ +(R_2+R_{22})T_1\left(\frac{\partial^2 w_0}{\partial x^2}\right)+A_{12}\frac{1}{r}\frac{\partial u_0}{\partial x}+A_{12}\frac{1}{r}\frac{1}{2}\left(\frac{\partial w_0}{\partial x}\right)^2\\ +A_{22}\frac{1}{r^2}w_0+B_{12}\frac{1}{r}\left(\frac{\partial \varphi_x}{\partial x}\right)-(R_1+R_{12})\frac{1}{r}T_0-(R_2+R_{22})\frac{1}{r}T_1\\ -A_{55}.\left(\frac{\partial^2 w_0}{\partial x^2}+\frac{\partial \varphi_x}{\partial x}\right)-I_1\frac{\partial^2 w_0}{\partial t^2}-K_L h w_0-K_{NL}h{w_0}^3=0\end{aligned} \tag{18}$$

Third equation of motion

$$-B_{11}.\frac{\partial^2 u_0}{\partial x^2}-B_{11}\left(\frac{\partial^2 w_0}{\partial x^2}\right)\left(\frac{\partial w_0}{\partial x}\right)-\frac{B_{12}}{r}\left(\frac{\partial w_0}{\partial x}\right)-D_{11}\left(\frac{\partial^2 \varphi_x}{\partial x^2}\right)+(R_2+R_{22})\left(\frac{\partial T_0}{\partial x}\right)+(R_3+R_{33})\left(\frac{\partial T_1}{\partial x}\right)+A_{55}\left(\frac{\partial w_0}{\partial x}+\varphi_x\right)-I_2\frac{\partial^2 u_0}{\partial t^2}-I_3\frac{\partial^2 \varphi_x}{\partial t^2}=0 \tag{19}$$

2.4 Energy equations

The classical theory of coupled thermoelasticity for the FG cylindrical shell is considered as [4]

$$\rho c_\varepsilon \dot{T}+\beta T_a \dot{\varepsilon}_{ii}=\left(kT_{,i}\right)_{,i} \tag{20}$$

Where ρ is the mass density, c_ϵ is the specific heat at constant strain, $\beta=\alpha(3\lambda+2\mu)$, T_a is the reference temperature, k is the heat conduction coefficient. This equation may be written in expanded form for the assumed conditions. We move all terms of the equation to the left side of the equation and calling it the residue $R(T)$. The resulting residue $R(T)$ is made orthogonal with respect to 1 and z. This yields two independent equations for T_0 and T_1, as it is made orthogonal with respect to 1 and z for T_0 and T_1 . Temperature distribution may be considered linear across the shell thickness as

$$T(x,\theta,z,t)-T_a=T_0(x,\theta,t)+zT_1(x,\theta,t) \tag{21}$$

The assumed temperature distribution is substituted into the energy equation [22] and the resulting residue $Re(T,z)$ is made orthogonal with respect to 1 and z. This yields two independent equations for T_0 and T_1 as

$$\begin{aligned} \int Re.dz &= 0 \\ \int Re.z.dz &= 0 \end{aligned} \tag{22}$$

The boundary conditions for energy equation are considered as

$$k(-h/2)\frac{\partial T}{\partial z}\Big|_{-\frac{h}{2}} = Q_i, \qquad z = -\frac{h}{2} \tag{23}$$

$$k(h/2)\frac{\partial T}{\partial z}\Big|^{\frac{h}{2}} = Q_o, \qquad z = \frac{h}{2} \tag{24}$$

$$k\frac{\partial T}{\partial x}\Big|_0 = 0, \qquad x = 0 \tag{25}$$

$$k\frac{\partial T}{\partial x}\Big|^{L} = 0, \qquad x = L \tag{26}$$

where L is the cylinder length and Q_i and Q_o are the heat flux applied to the inside and outside shell surfaces, respectively. The two energy equations in terms of the displacement components are written as follow. The coefficients are given in the Appendix.
First:

$$\begin{aligned} &\left[T_a(R_1+R_{12})\left(\frac{\partial^2}{\partial x\,\partial t}\right)\right]u_0 + \frac{1}{2}\left[T_a(R_1+R_{12})\left(\frac{\partial}{\partial t}\right)\right](w_{0,x})^2 \\ &+\left[T_a(R_1+R_{12})\frac{1}{r}\left(\frac{\partial}{\partial t}\right)\right]w_0 + \left[T_a(R_2+R_{22})\left(\frac{\partial^2}{\partial x\,\partial t}\right)\right]\varphi_x \\ &+\left[C_{11}.\left(\frac{\partial}{\partial t}\right) - K_1.\frac{\partial^2}{\partial x^2}\right]T_0 + \left[C_{22}.\left(\frac{\partial}{\partial t}\right) - K_2.\frac{\partial^2}{\partial x^2}\right]T_1 \\ &= Q_o - Q_i \end{aligned} \tag{27}$$

Second:

$$\begin{aligned} &\left[T_a(R_2+R_{22})\left(\frac{\partial^2}{\partial x\,\partial t}\right)\right]u_0 + \frac{1}{2}\left[T_a(R_2+R_{22})\left(\frac{\partial}{\partial t}\right)\right](w_{0,x})^2 \\ &+\left[T_a(R_2+R_{22})\frac{1}{r}\left(\frac{\partial}{\partial t}\right)\right]w_0 + \left[T_a(R_3+R_{32})\left(\frac{\partial^2}{\partial x\,\partial t}\right)\right]\varphi_x \\ &+\left[C_{22}.\left(\frac{\partial}{\partial t}\right) - K_2.\frac{\partial^2}{\partial x^2}\right]T_0 + \left[C_{33}\left(\frac{\partial}{\partial t}\right) - K_3.\frac{\partial^2}{\partial x^2} + K_1\right]T_1 \\ &= \frac{h}{2}(Q_o + Q_i) \end{aligned} \tag{28}$$

The resulting energy equations, as given by Eqs, [26] and [27], are nonlinear due to the assumed nonlinear kinematical relation.

The simultaneous solution of the nonlinear equations of motion and nonlinear energy equations provide a system of equations to be used to determine the vibrations of the shell under the applied thermal shock load and with elastic foundation. This system of equations involves five unknown functions u_0, w_0, φ_x, T_0, and T_1 as functions of time for the coupled thermoelasticity problem of functionally graded cylindrical shell.

A numerical technique is used to solve the governing equations in time domain and the Galerkin finite element method employed to obtain the solution in the space domain. Before solving the problem, the governing equations are made dimensionless. For this purpose, the following dimensionless parameters are defined [4]

dimensionless length:

$$\bar{\mathrm{x}} = \frac{x}{L} \tag{29}$$

dimensionless time:

$$\bar{t}_0 = \frac{t_0 C_1}{L}, \quad \bar{t} = \frac{tC_1}{L} \tag{30}$$

dimensionless temperature:

$$\Delta\bar{\mathrm{T}} = \frac{T - T_a}{T_a}\bar{T}_0 = \frac{T_0}{T_a}\bar{T}_1 = \frac{LT_1}{T_a} \tag{31}$$

dimensionless displacement field:

$$\bar{u}_0 = \frac{(\lambda_m + 2\mu_m)u_0}{L\gamma_m T_a}, \qquad \bar{w}_0 = \frac{(\lambda_m + 2\mu_m)w_0}{L\gamma_m T_a}, \qquad \bar{\varphi}_x = \frac{(\lambda_m + 2\mu_m)\varphi_x}{\gamma_m T_a} \tag{32}$$

dimensionless stress:

$$\bar{\sigma}_{ij} = \frac{\sigma_{ij}}{\gamma_m T_a} \tag{33}$$

Where

$$\mathrm{L} = \frac{\mathrm{k_m}}{\rho_m C_m C_1} \tag{34}$$

$$C_1 = \sqrt{\frac{\lambda_m + 2\mu_m}{\rho_m}} \tag{35}$$

and γ_m, λ_m, μ_m, ρ_m, c_m, k_m, and υ are the metal physical constants.

2.5 Finite Element Method

The dimensionless equations of motion and energy are solved with the Galerkin method in space domain and Newmark method in time domain. The linear shape function is employed to model the finite element equations. Proper explanations for the accuracy and convergence of this model is provide by Hetnarski and Eslami in reference.
Due to the assumed symmetric thermal loading condition, only the longitudinal element is required. Calling the element function $\phi^{(e)}$ along the longitudinal direction, the variation in the base element (e) is

$$\phi^{(e)} = N_i\phi_i + N_j\phi_j \tag{36}$$

and the shape functions in terms of the local coordinate ξ are

$$\{N\} = \begin{Bmatrix} N_i \\ N_j \end{Bmatrix} = \begin{Bmatrix} \frac{1}{2}(1-\xi) \\ \frac{1}{2}(1+\xi) \end{Bmatrix}$$

The variations of the unknown functions involved in the governing equations in the base element (e) are

$$\begin{aligned}
\bar{u}_0(x,t) &=< N_{u0i} \quad N_{u0j} > \begin{Bmatrix} U_{0i}(t) \\ U_{0j}(t) \end{Bmatrix} \\
\bar{w}_0(x,t) &=< N_{w0i} \quad N_{w0j} > \begin{Bmatrix} W_{0i}(t) \\ W_{0j}(t) \end{Bmatrix} \\
\bar{\varphi}_x(x,t) &=< N_{\varphi xi} \quad N_{\varphi xj} > \begin{Bmatrix} \phi_{xi}(t) \\ \phi_{xj}(t) \end{Bmatrix} \\
T_0(x,t) &=< N_{T_{0i}} \quad N_{T_{0j}} > \begin{Bmatrix} T_{T0i}(t) \\ T_{T0j}(t) \end{Bmatrix} \\
\bar{T}_1(x,t) &=< N_{T_{1i}} \quad N_{T_{1j}} > \begin{Bmatrix} T_{T1i}(t) \\ T_{T1j}(t) \end{Bmatrix}
\end{aligned}$$

The dimensionless nonlinear equations of motion and energy, employing the assumed shape functions given above and proper weak formulations for the coupled problem [22], are written as

$$\begin{aligned}
&\int_{-1}^{1} \Big(\frac{2A_{11}}{(\lambda_m+2\mu_m)L} \frac{\partial N_{u0l}}{\partial \xi} \frac{\partial N_{u0}}{\partial \xi} U_0(t) + \frac{2\gamma_m T_a A_{11}}{(\lambda_m+2\mu_m)^2 L} \frac{\partial N_{u0l}}{\partial \xi} \frac{\partial N_{w0}}{\partial \xi} W_0(t) \frac{\partial N_{w0}}{\partial \xi} W_0(t) \\
&+ \frac{A_{12}}{(\lambda_m+2\mu_m)r} \frac{\partial N_{u0l}}{\partial \xi} N_{w0} W_0(t) + \frac{2B_{11}}{(\lambda_m+2\mu_m)L^2} \frac{\partial N_{u0l}}{\partial \xi} \frac{\partial N_{\varphi x}}{\partial \xi} \phi_x(t) \\
&- \frac{(R_1+R_{12})}{\gamma_m L} \frac{\partial N_{u0l}}{\partial \xi} N_{T0} T_{T0}(t) - \frac{(R_2+R_{22})}{\gamma_m L^2} \frac{\partial N_{u0l}}{\partial \xi} N_{T1} T_{T1}(t) \\
&+ \frac{I_1}{2\rho_m L} N_{u0l} N_{u0} \frac{\partial^2 U_0(t)}{\partial \bar{t}^2} + \frac{I_2}{2\rho_m L^2} N_{u0l} N_{\varphi x} \frac{\partial^2 \phi_x(t)}{\partial \bar{t}^2} \Big) d\xi = -N_{u0l} \bar{N}_{xx} \Big|_{-1}^{1}
\end{aligned} \tag{37}$$

$$\int_{-1}^{1}\Bigg(\frac{A_{12}}{(\lambda_m+2\mu_m)r^2}\frac{\partial N_{w0l}}{\partial\xi}N_{u0}U_0(t)+\frac{4\gamma_m T_a A_{11}}{(\lambda_m+2\mu_m)^2 L}\frac{\partial N_{w0l}}{\partial\xi}\frac{\partial N_{w0}}{\partial\xi}W_0(t)\frac{\partial N_{u0}}{\partial\xi}U_0(t)$$
$$+\frac{2\gamma_m T_a A_{12}}{(\lambda_m+2\mu_m)^2 r}\times\frac{\partial N_{w0l}}{\partial\xi}N_{w0}W_0(t)\frac{\partial N_{w0}}{\partial\xi}W_0(t)$$
$$+\frac{\gamma_m T_a A_{12}}{(\lambda_m+2\mu_m)^2 r}N_{w0l}\frac{\partial N_{w0}}{\partial\xi}W_0(t)\frac{\partial N_{w0}}{\partial\xi}W_0(t)$$
$$+\frac{2A_{55}}{(\lambda_m+2\mu_m)L}\frac{\partial N_{w0l}}{\partial\xi}\frac{\partial N_{w0}}{\partial\xi}W_0(t)+\frac{A_{22}L}{2(\lambda_m+2\mu_m)r^2}N_{w0l}N_{w0}W_0(t)$$
$$+\frac{4A_{11}(\gamma_m T_a)^2}{(\lambda_m+2\mu_m)^3 L}\frac{\partial N_{w0l}}{\partial\xi}\frac{\partial N_{w0}}{\partial\xi}W_0(t)\frac{\partial N_{w0}}{\partial\xi}W_0(t)\frac{\partial N_{w0}}{\partial\xi}W_0(t)$$
$$+\frac{4B_{11}\gamma_m T_a}{(\lambda_m+2\mu_m)^2 L^2}\frac{\partial N_{w0l}}{\partial\xi}\frac{\partial N_{w0}}{\partial\xi}W_0(t)\frac{\partial N_{\varphi x}}{\partial\xi}\phi_x(t)$$
$$+\frac{A_{55}}{(\lambda_m+2\mu_m)L}\frac{\partial N_{w0l}}{\partial\xi}N_{\varphi x}\phi_x(t)+\frac{B_{12}}{(\lambda_m+2\mu_m)rL}N_{w0l}\frac{\partial N_{\varphi x}}{\partial\xi}\phi_x(t)$$
$$-\frac{(R_1+R_{12})}{2\gamma_m r}N_{w0l}N_{T0}T_{T0}(t)-\frac{(R_2+R_{22})}{2\gamma_m rL}N_{w0l}N_{T1}T_{T1}(t)$$
$$-\frac{I_1}{2\rho_m L}N_{w0l}N_{w0}\frac{\partial^2 W_0(t)}{\partial\bar{t}^2}-K_L\frac{h}{2(\lambda_m+2\mu_m)}N_{w0l}N_{w0}W_0(t)$$
$$-K_{NL}\frac{L^2{\gamma_m}^2{T_a}^2 h}{(\lambda_m+2\mu_m)^3}N_{w0l}N_{w0}W_0(t)N_{w0}W_0(t)N_{w0}W_0(t)\Bigg)\,d\xi$$
$$=-N_{w0l}\bar{Q}_x\Big|_{-1}^{1}-\left(\frac{2\gamma_m T_a}{(\lambda_m+2\mu_m)}\right)N_{w0l}\frac{\partial N_{w0}}{\partial\xi}W_0(t).\bar{N}_{xx}\Big|_{-1}^{1} \tag{38}$$

$$\int_{-1}^{1}\Bigg(\frac{2B_{11}}{(\lambda_m+2\mu_m)L^2}\frac{\partial N_{x\varphi l}}{\partial\xi}\frac{\partial N_{u0}}{\partial\xi}U_0(t)$$
$$+\frac{2\gamma_m T_a B_{11}}{(\lambda_m+2\mu_m)^2 L^2}\frac{\partial N_{\varphi xl}}{\partial\xi}\frac{\partial N_{w0}}{\partial\xi}W_0(t)\frac{\partial N_{w0}}{\partial\xi}W_0(t)$$
$$+\frac{B_{12}}{(\lambda_m+2\mu_m)Lr}\frac{\partial N_{\varphi xl}}{\partial\xi}N_{w0}W_0(t)+\frac{A_{55}}{(\lambda_m+2\mu_m)L}N_{\varphi xl}\frac{\partial N_{w0}}{\partial\xi}W_0(t)$$
$$+\frac{2D_{11}}{(\lambda_m+2\mu_m)L^3}\frac{\partial N_{\varphi xl}}{\partial\xi}\frac{\partial N_{\varphi x}}{\partial\xi}\phi_x(t)+\frac{A_{55}}{2(\lambda_m+2\mu_m)L}N_{\varphi xl}N_{\varphi x}\phi_x(t)$$
$$-\frac{(R_2+R_{22})}{\gamma_m L^2}\frac{\partial N_{\varphi xl}}{\partial\xi}N_{T0}T_{T0}(t)-\frac{(R_3+R_{32})}{\gamma_m L^3}\frac{\partial N_{\varphi xl}}{\partial\xi}N_{T1}T_{T1}(t)$$
$$+\frac{I_2}{2\rho_m L^2}N_{\varphi xl}N_{u0}\frac{\partial^2 U_0(t)}{\partial\bar{t}^2}+\frac{I_3}{2\rho_m L^3}N_{\varphi xl}N_{\varphi x}\frac{\partial^2\phi_x(t)}{\partial\bar{t}^2}\Bigg)d\xi$$
$$=-N_{\varphi xl}\bar{M}_{xx}\Big|_{-1}^{1} \tag{39}$$

$$\int_{-1}^{1} \frac{(R_1+R_{12})T_a}{(\lambda_m+2\mu_m)L^2} N_{T0l} \frac{\partial N_{u0}}{\partial \xi} \frac{\partial U_0(t)}{\partial \bar{t}}$$
$$+ \frac{(R_1+R_{12})2{T_a}^2\gamma_m}{(\lambda_m+2\mu_m)^2L^2} N_{T0l} \frac{\partial N_{w0}}{\partial \xi} W_0(t) \frac{\partial N_{w0}}{\partial \xi} \frac{\partial W_0(t)}{\partial \bar{t}}$$
$$+ \frac{(R_1+R_{12})T_a}{(\lambda_m+2\mu_m)2r} N_{T0l} N_{w0} \frac{\partial W_0(t)}{\partial \bar{t}} + \frac{(R_2+R_{22})T_a}{(\lambda_m+2\mu_m)L^2} N_{T0l} \frac{\partial N_{\varphi x}}{\partial \xi} \frac{\partial \phi_x(t)}{\partial \bar{t}}$$
$$+ \frac{C_{11}}{\gamma_m} \frac{1}{2L} N_{T0l} N_{T0} \frac{\partial T_{T0}(t)}{\partial \bar{t}} + \frac{C_{22}}{\gamma_m} \frac{1}{2L^2} N_{T0l} N_{T1} \frac{\partial T_{T1}(t)}{\partial \bar{t}} \tag{40}$$
$$+ \frac{2K_2}{\gamma_m C_1 L^2} \frac{\partial N_{T0l}}{\partial \xi} \frac{\partial N_{T0}}{\partial \xi} T_{T0}(t) + \frac{2K_1}{\gamma_m C_1 L^3} \frac{\partial N_{T0l}}{\partial \xi} \frac{\partial N_{T1}}{\partial \xi} T_{T1}(t)) d\xi$$
$$= \frac{1}{\gamma_m T_a L^2 C_1} \left(\int_{-1}^{1} N_{T0l}(Q_o - Q_i) \frac{L}{2} d\xi + N_{T0l} \left(\int K(z) \frac{\partial T}{\partial \xi} dz) \right|_{-1}^{1} \right)$$

$$\int_{-1}^{1} \frac{(R_2+R_{22})T_a}{(\lambda_m+2\mu_m)L^2} N_{T1l} \frac{\partial N_{u0}}{\partial \xi} \frac{\partial U_0(t)}{\partial \bar{t}}$$
$$+ \frac{(R_2+R_{22})2{T_a}^2\gamma_m}{(\lambda_m+2\mu_m)^2L^2} N_{T1l} \frac{\partial N_{w0}}{\partial \xi} W_0(t) \frac{\partial N_{w0}}{\partial \xi} \frac{\partial W_0(t)}{\partial \bar{t}}$$
$$+ \frac{(R_2+R_{22})T_a}{(\lambda_m+2\mu_m)2Lr} N_{T1l} N_{w0} \frac{\partial W_0(t)}{\partial \bar{t}}$$
$$+ \frac{(R_3+R_{32})T_a}{(\lambda_m+2\mu_m)L^3} N_{T1l} \frac{\partial N_{\varphi x}}{\partial \xi} \frac{\partial \phi_x(t)}{\partial \bar{t}} + \frac{C_{22}}{\gamma_m} \frac{1}{2L^2} N_{T1l} N_{T0} \frac{\partial T_{T0}(t)}{\partial \bar{t}} \tag{41}$$
$$+ \frac{C_{33}}{\gamma_m} \frac{1}{2L^3} N_{T1l} N_{T1} \frac{\partial T_{T1}(t)}{\partial \bar{t}} + \frac{2K_2}{\gamma_m C_1 L^2} \frac{\partial N_{T1l}}{\partial \xi} \frac{\partial N_{T0}}{\partial \xi} T_{T0}(t)$$
$$+ \frac{2K_3}{\gamma_m C_1 L^3} \frac{\partial N_{T1l}}{\partial \xi} \frac{\partial N_{T1}}{\partial \xi} T_{T1}(t)) d\xi$$
$$= \frac{1}{\gamma_m T_a L^2 C_1} \left(\int_{-1}^{1} N_{T1l}.(Q_o - Q_i) \frac{hL}{4} d\xi + N_{T1l} \left(\int K(z) z \frac{\partial T}{\partial \xi} dz) \right|_{-1}^{1} \right)$$

where l = I, j. Note that in the above equations the following matrix notations are considered. Here, Q_i and Q_o are the inner and outer non-dimension applied heat flux and K_L and $K_{\{NL\}}$ are winkler coefficients.

$$U_0(t) = \begin{Bmatrix} U_{0i}(t) \\ U_{0j}(t) \end{Bmatrix}$$

$$W_0(t) = \begin{Bmatrix} W_{0i}(t) \\ W_{0j}(t) \end{Bmatrix}$$
$$\phi_x(t) = \begin{Bmatrix} \phi_{xi}(t) \\ \phi_{xj}(t) \end{Bmatrix}$$
$$T_{T0}(t) = \begin{Bmatrix} T_{T0i}(t) \\ T_{T0j}(t) \end{Bmatrix}$$
$$T_{T1}(t) = \begin{Bmatrix} T_{T1i}(t) \\ T_{T1j}(t) \end{Bmatrix}$$

and

$$\begin{aligned} N_{\{uo\}} &=< N_{\{u0i\}} \quad N_{\{u0j\}} > \\ N_{\{wo\}} &=< N_{\{w0i\}} \quad N_{\{w0j\}} > \\ N_{\{\varphi_x\}} &=< N_{\{\varphi_{xi}\}} \quad N_{\{\varphi_{xj}\}} > \\ N_{\{T_0\}} &=< N_{\{T_{0i}\}} \quad N_{\{T_{0j}\}} > \\ N_{\{T_1\}} &=< N_{\{T_{1i}\}} \quad N_{\{T_{1j}\}} > \end{aligned} \tag{42}$$

The set of equations given by Eqs. [37] to [41] for the base element \left(e\right) with nodes i and j are assembled for all elements in the solution domain to receive at the following general nonlinear finite element equation.

$$[M]\{\ddot{X}\} + [C(X)]\{\dot{X}\} + [K(X)]\{\mathrm{X}\} = \{\mathrm{F}(t)\} \tag{43}$$

It is noted that due to the nonlinear nature of the governing finite element equations, capacitance, and stiffness matrices $[C]$, and $[K]$ are variable dependent

2.6 Numerical method

Due to the nonlinearity of the governing equations and coupling of the displacement terms and their derivatives in these equations, an incremental solution method is adopted to check the thermal stability of the shell.

The nonlinear finite element equation (43) is solved by time marching method assuming that the initial conditions$\dot{X}_0$and X_0 are given [23, 24]. The force function $\{\mathrm{F}\}$ is the assumed thermal shock load known in terms of time and is given at any step time. The numerical solution is accomplished through the following steps [25].

- Step 1. The cylindrical shell is discretized into a number of elements along the axial direction with axisymmetric assumption.
- Step 2. The initial values of the middle surface displacement components, rotation, and temperatures T_0 and T_1 in the unknown matrix $\{X_0\}$ are set to zero. The initial first time rate of these functions, $\dot{X}_0$, are also set equal to zero.
- Step 3. The mass, stiffness, and capacitance matrices are calculated using the initial values of mid-plane displacement components give in step 2.
- Step 4. The matrix $\{\ddot{\mathrm{X}}_0\}$ is calculated from Eq. (43) using the mass, stiffness, and capacitance matrices with the given $\{\dot{\mathrm{X}}_0\}$ and X_0.

$$[M]\{\ddot{X}\} + [C(X)]\{\dot{X}\} + [K(X)]\{\mathrm{X}\} = \{\mathrm{F}(t)\} \tag{44}$$

- Step 5. Time is incremented. Choosing $\Delta t$and calculating $t_{\{n+1\}} = \Delta \mathrm{t} + t_n$, where n is the step time counter.
- Step 6. Calculating the Newmark integration constants according to the following equations. Two parameters γ and β are selected. The parameter $\gamma = \frac{1}{2}$ ensures second order accuracy and $\beta = \frac{1}{4}$ makes the algorithm implicit and equivalent to the trapezoidal rule [22].

$$\begin{aligned} a_1 &= \frac{[M]}{\beta \Delta t^2} + \gamma \frac{[C]}{\beta \Delta t} \\ a_2 &= \frac{[M]}{\beta \Delta t} + \left(\frac{\gamma}{\beta} - 1\right)[C] \\ a_3 &= \left(\frac{1}{2\beta} - 1\right)[M] + \Delta t \left(\frac{\gamma}{2\beta} - 1\right)[C] \\ \left[\tilde{K}\right] &= [K] + a_1 \end{aligned} \tag{45}$$

- Step 7. Calculating the equivalent stiffness and force matrices]K̃] and]F̃] and predicting with assumption $\{\mathrm{X}\}_{\{n+1\}} = \{\mathrm{X}\}_n$.

$$\{\tilde{F}\}_{\mathrm{n+1}} = \{\mathrm{F}\}_{\mathrm{n+1}} + a_1 \times \{\mathrm{X}\}_n + a_2 \times \frac{\partial \{\mathrm{x}\}_{\mathrm{n}}}{\partial \mathrm{t}} + a_3 \times \frac{\left\{\partial_n^{2\{X\}}\right\}}{\{\partial t^2\}} \tag{46}$$

$$\left[\tilde{\mathrm{K}}\right]_{\mathrm{n+1}} = K_{\{n+1\}} + a_1 \tag{47}$$

- Step 8. Calculate the residual vector

$$\left\{\tilde{\mathrm{R}}\right\}_{n+1} = \{\tilde{F}\}_{n+1} - [K(X_{n+1})]\{X\}_{n+1} - a_1 \times \{X\}_{n+1} \tag{48}$$

- Step 9. Solve the term Δ{X} from the equation

$$\Delta\{\mathrm{x}\} = \frac{\left\{\tilde{\mathrm{R}}_{n+1}\right\}}{\left[\tilde{K}\right]_{n+1}} \tag{49}$$

- Step 10. If $|\Delta\{\mathrm{X}\}| \leq \{\eta\}$, $\{\eta\}$ being the convergence parameter vector, calculate the velocity and acceleration vectors from the next step.
- Step 11. Calculate the nodes velocity $\{\dot{X}\}$ and acceleration $\{\ddot{X}\}$from the following equations and enter them into the next time step.

$$\frac{\mathrm{d}\{\mathrm{X}\}_{\mathrm{n+1}}}{dt} = \gamma \frac{\{X\}_{n+1} - \{X\}_n}{\beta \Delta t} + \left(1 - \frac{\gamma}{\beta}\right)\frac{d\{X\}_n}{dt} + \Delta t \left(1 - \frac{\gamma}{2\beta}\right)\frac{d^2\{X\}_n}{dt^2} \tag{46}$$

$$\frac{\mathrm{d}^2\{X\}_{n+1}}{dt^2} = \frac{\{X\}_{n+1} - \{X\}_n}{\beta \Delta t^2} + \frac{1}{\beta \Delta}\frac{d\{X\}_n}{dt} + \Delta t \left(1 - \frac{\gamma}{2\beta}\right)\frac{d^2\{X\}_n}{dt^2} \tag{47}$$

- Step 12. If$|\Delta\{X\}| > \{\eta\}$, we consider $\Delta\{\mathrm{X}\}^m$ instead of$\Delta\{\mathrm{X}\}$, where m is the iteration counter and

$$\Delta\{\mathrm{X}\}^m = \{\mathrm{X}\}_{\{n+1\}}^{\{m+1\}} - \{\mathrm{X}\}_{\{n+1\}}^{m}$$

- Step 13. Calculate $\{\mathrm{X}\}_{\{n+1\}}^{\{m+1\}}$ from the above equation, where $\{\mathrm{X}\}_{\{n+1\}}^{m}$ at the first iteration is equal to $\{\mathrm{X}\}_{\{n+1\}}^{1}$ or $\{\mathrm{X}\}_{\{n+1\}}$ predicted in step 7.
- Step 14. Recalculate $\{\widetilde{\mathrm{R}}\}_{\{n+1\}}$ and $\left[\widetilde{\mathrm{K}}\right]_{n+1}$with $\{\mathrm{X}\}_{\{n+1\}}^{\{m+1\}}$.
- Step 15. Calculate $\Delta\{\mathrm{X}\}$ with new $\left\{\widetilde{\mathrm{R}}\right\}_{n+1}$and $\left[\widetilde{K}\right]_{n+1}$and check the convergence. If converged, go to step 11 otherwise go to step 12 for the next iteration m.

3 Results

The formulations and method of solution derived in this research are validated with those reported byBahtui and Eslami. For the comparison with this reference, the displacement fields are calculated based on the linear coupled thermoelasticity of the FG cylindrical shell by eliminating the nonlinear terms in the strain-displacement relations. The dimensions of the cylindrical shell, material, boundary conditions, thermal shock, and dimensionless methods are selected similar to those used in Behtui and Eslamiarticle.
The radial displacement versus time at the middle length of the functionally graded cylindrical shell is presented in Fig. (2) The material is Ti6Al4V/ZrO_2 and the power law index is selected equal to zero. Similar to reference, the clamped cylindrical shell under inside impulsive thermal shock load is considered. The ratio of length of shell to radius is equal to 5 and the ratio $\frac{\mathrm{R}}{\mathrm{h}}$ is 10, where h and R are the thickness and radius of the shell, respectively. The equation of thermal shock similar to reference is:

$$\mathrm{T}(t) = 2201.85 \times a\mathrm{T}e^{\{-13100bt\}} + 298.15$$

wherea and b are selected such that the impulsive shock period becomes $\{10\}^{\{-6\}}$ s and $\mathrm{T}(t)$ is the time dependent temperature. This equation generates a convective heat flux equal to $2201.85 \times \frac{h_{\{in\}\backslash\mathrm{times}W}}{m^2}$ in $0.5\backslash mus$. The thermal boundary conditions at the ends of the shell are assumed to be insulated. The coefficient of thermal convection of the ceramic-rich inside surface is ($h_{\{in\}}$ = 10,000 $\frac{\mathrm{W}}{m^2}$ K) and that of the metal rich outside surface is ($h_{\{out\}}$ = 200 $\frac{\mathrm{W}}{m^2}$ K). The comparison shown in Fig. (2) is well justified.

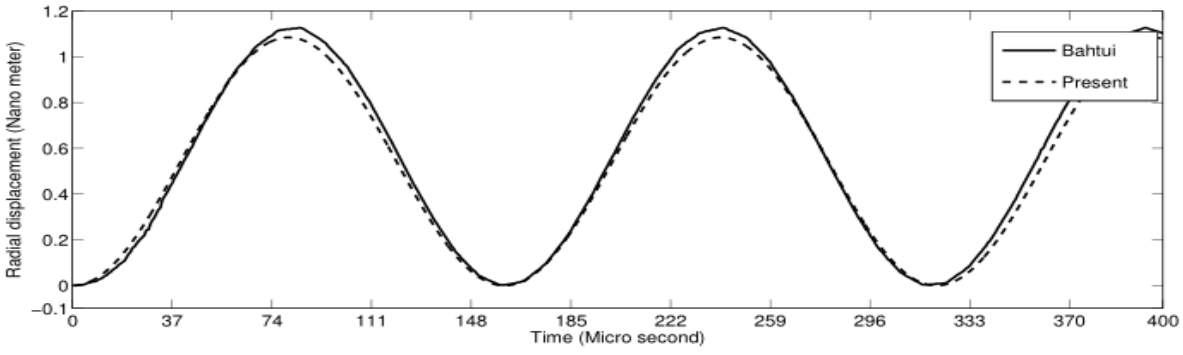

Figure 2 Comparison between the radial displacement of middle length of the shell versus time with that reported in [5].

Table 1 Material properties of FGM

Metal		Ceramics	
$\mathrm{E}(Gpa)$	66.2	E	117
υ	0.327	υ	0.327
$\alpha(1/K)$	$7.11 * \{10\}^{\{-6\}}$	α	$18.48 * \{10\}^{\{-6\}}$
$\rho(\mathrm{kg/m^3})$	$8.9 * \{10\}^3$	ρ	$2.37 * \{10\}^3$
K(W/mK)	6.08	K	1.775
c (J/kgK)	625	c	529

The aim of this research is to check the effect of elastic foundation around shells under an applied thermal shock load and check the vibrations of shell with several thickness to radius ratios and length to shell diameter ratios.

Now, consider a simply supported functionally graded cylindrical shell under the outside impulsive thermal shock. The ratio of the length to cylinder diameter is assumed to be 2, and the ratio $\frac{\mathrm{R}}{\mathrm{h}}$ is considered to be 15. The functionally graded shell is assumed to be made of combination of metal (Ti–6Al–4V) and ceramic (ZrO2), at the initial temperature 298.15 K, with the material properties given in Table (1) . The shell is ceramic-rich in inside and metal-rich at outside surfaces, respectively. The same boundary conditions at both ends of the cylindrical shell are considered.

Consider the linear and nonlinear winkleer elastic foundation coefficients $K_L$and $K_{\{NL\}}$. Here, the dimensionless coefficients are $\bar{K}_L$and $\bar{K}_{NL}$. The functionally graded shell is studied for the power law indices of i = 0 and i=10, for a metal or almost pure ceramic shell. The plots of radial displacement versus time for different values of the Winkler coefficients are presented in the following figures. The response of the shell for thermal shock condition with several thickness to radius ratios and length to shell diameter ratios are studied. The thermal shock load is considered in form of $\mathrm{Q} = \mathrm{A}\bar{t}^3 e^{-B\bar{t}}$ heat flux applied to the outside surface of the shell, where A and B are some constant parameters. The thermal shock load, calling Q, is selected with values A=960 and B=0.55. The time period of Q is less than the lowest natural frequency of the shell.

Figure (3) shows the radial displacement of middle length of the shell versus time (150 dimensionless time) with several Winkler coefficients under the shock load Q, when the power law index (i) is equal to 10 with the assumption of nonlinear strain-displacement relations. Radial response of the shell is stable, vibratory, with small time periods, and follows a long range vibrations as time advances.

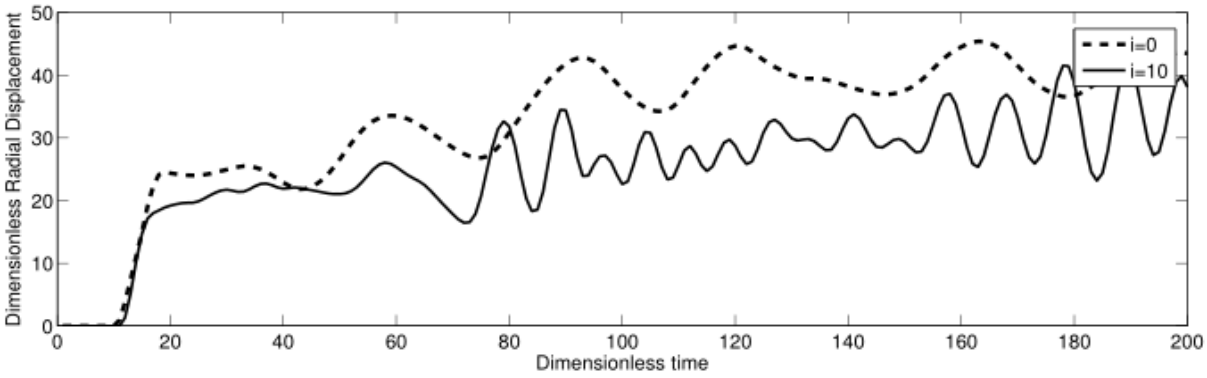

Figure 3 Radial displacement of middle length of the shell versus time with several Winkler coefficients, considering the nonlinear strain-displacement relations and i =10.

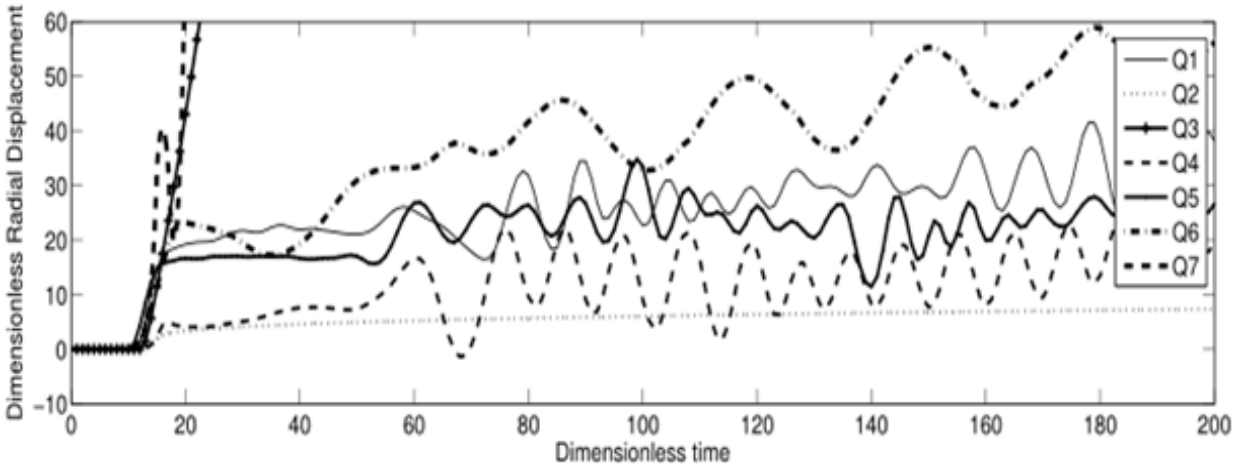

Figure 4 Radial displacement of middle length of the shell versus time under the shock Q and power law indices 0 and 10, considering the nonlinear strain-displacement relations

The amplitudes for lower Winkler coefficients is larger compared to larger coefficients, where $K_{\{L1\}} = K_{NL1} = 0$, $K_{\mathrm{L2}} = 2 \times 10^7\ N/m^3$, $K_{NL2} = 7.5 \times 10^{11}\ N/m^5$, and $K_{L3} = 2 \times 10^8\ N/m^3$, $K_{NL3} = 7.5 \times 10^{12}\ N/m^5$. Here the power law index is equal to $\mathrm{i} = 10$ which shows that the shell is almost pure ceramic. When the Winkler coefficient increases, the stiffness of the foundation increases and the shell becomes more resistant to deformations. In the first curve, the linear and nonlinear Winkler coefficients are considered to be zero ($K_{N1} = K_{NL1} = 0$). In the second curve, non-zero Winkler coefficients are considered, and are assumed to be $K_{N3}/K_{N2} = K_{NL3}/K_{NL2} = 10$. In the third curve, the Winkler coefficients are considered 10 times larger than the second case.

Figure (4) shows the radial displacement of middle length of the shell versus time (150 dimensionless time) under the shock load Q, when the power law index (i)is equal to zero and 10 with the assumption of nonlinear strain-displacement relations, where the Winkler coefficients are equal to $K_L = 2 \times 10^7\ N\backslash m^3$and $K_{NL} = 7.5 \times 10^{11}\ N/m^5$. The problem is solved with these coefficients and is shown in the second curve of Figure (3). Radial response of the shell is stable, vibratory, with small time periods and follow a long-range vibration as time advances. The amplitudes for the power law index $\mathrm{i} = 0$ is larger compared to $\mathrm{i} = 10$, as the power law index $\mathrm{i} = 0$ represents pure metal with lower modulus of elasticity compared to the ceramic for larger power law indices of the FGM shell. As the power law index increases, the material changes from metal state to a combination of ceramic and metal.

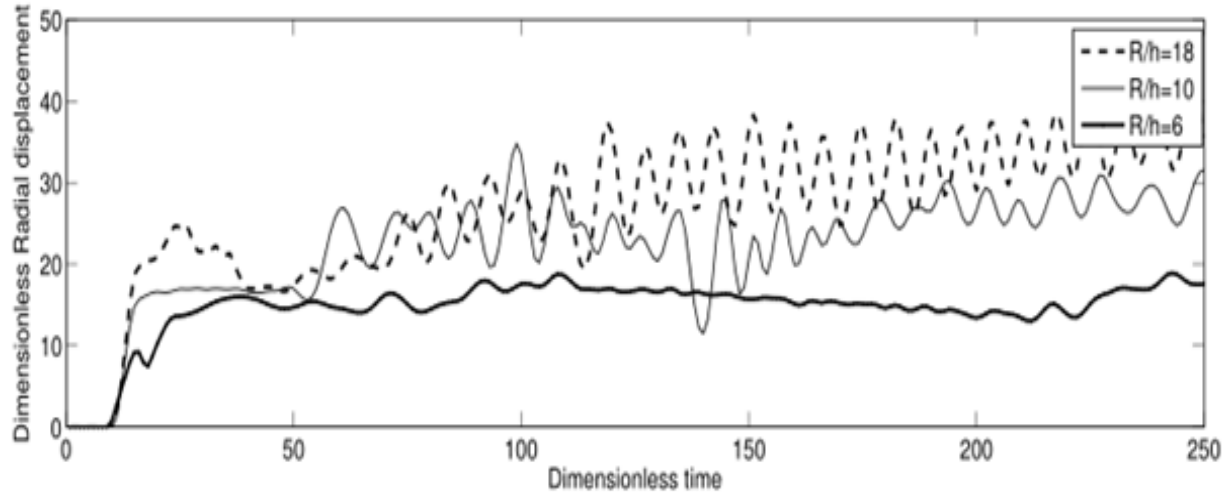

Figure 5 Radial displacement of middle length of the shell versus time for different R/h ratios and i=10.

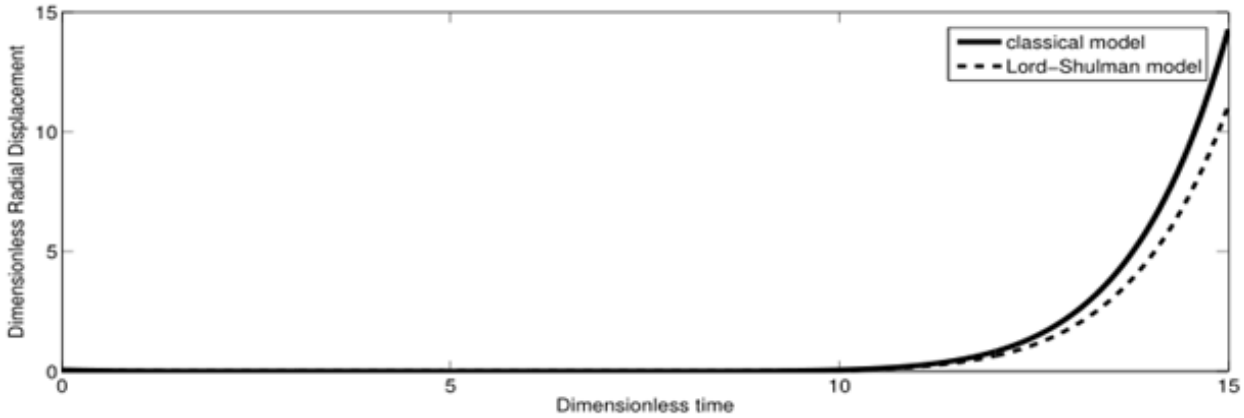

Figure 6 Radial displacement of middle length of the shell versus time for different L/D ratios and i=10.

In this condition and under the same thermal shock load, the amplitude of vibrations decrease and the frequency of vibrations increase with the increase of the power law index. Here, the radius to thickness of shell ratio is equal to 15 and length to diameter ratio is equal to 2.
Figure (5) shows the radial displacement of middle length of the shell versus time under the thermal shock load. This figure shows the radial displacement for different ratios of radius to shell thickness. The figure indicates that when ratio of radius to shell thickness increases the amplitude of vibrations increase too for different Winkler coefficients. This figure shows that there is a possibility of buckling as a result of reducing the thickness to radius ratio.
Figure (6) shows the radial displacement of middle length of the shell versus time under the thermal shock load. This figure shows the radial displacement for different ratios of shell length to shell thickness. The figure indicates that when ratio of shell length to shell diameter increases the amplitude of vibrations increase too for different Winkler coefficients. This figure shows that there is a possibility of buckling too as a result of increasing the shell length to shell diameter.

4 Conclusion

The coupled thermoelasticity theory is formulated employing the nonlinear strain-displacement relations. When the coupled assumption is considered, all the governing equations, including the energy equation, become nonlinear where the solution of which is complicated. The analysis presented in this article provides a method to handle the mathematical complexity of the problem.
The article presents the analysis of cylindrical shell resting on elastic foundation under impulsive thermal shock load. When the Winkler coefficients increase, the radial displacement of cylindrical shell decreases. In this condition, the stiffness of shell increases. Here, a comparison is made between the results of the several shell geometrical dimensions. The amplitude of vibrations decrease and the frequency of vibrations increase with the increase of the power law index. The amplitude of vibrations increase with the increase of shell length to shell diameter ratios. The amplitude of vibrations increase with the decrease of shell thickness to shell radius ratios too. How about the Winkler effectthe main issue in this paper is the effect of elastic foundation

References

[1] S. Bochkarev, "Free Vibrations of a Cylindrical Shell Partially Resting on Elastic Foundation," *Journal of Applied Mechanics and Technical Physics,* Vol. 59, pp. 1242-1250, 2018, doi: https://doi.org/10.1134/S0021894418070039.

[2] D. Paliwal and R. K. Pandey, "The Free Vibration of a Cylindrical Shell on an Elastic Foundation," 1998, doi: https://doi.org/10.1115/1.2893828.

[3] A. Sofiyev, "Large Amplitude Vibration of FGM Orthotropic Cylindrical Shells Interacting with the Nonlinear Winkler Elastic Foundation," *Composites Part B: Engineering*, Vol. 98, pp. 141-150, 2016, doi: https://doi.org/10.1016/j.compositesb.2016.05.018.

[4] Hetnarski, R.B., and Eslami, M.R., *Thermal Stresses – Advanced Theory and Applications*, Second Edition,Switzerland, Springer, 2019, https://doi.org/10.1007/978-3-030-10436-8.

[5] A. Bahtui and M. Eslami, "Coupled Thermoelasticity of Functionally Graded Cylindrical Shells," *Mechanics Research Communications*, Vol. 34, No. 1, pp. 1-18, 2007, doi: https://doi.org/10.1016/j.mechrescom.2005.09.003.

[6] M. Eslami, M. Shakeri, and R. Sedaghati, "Coupled Thermoelasticity of an Axially Symmetric Cylindrical Shell," *Journal of Thermal Stresses*, Vol. 17, No. 1, pp. 115-135, 1994, https://doi.org/10.1080/01495739408946250.

[7] A. Bahtui and M. Eslami, "Generalized Coupled Thermoelasticity of Functionally Graded Cylindrical Shells," *International Journal for Numerical Methods in Engineering*, Vol. 69, No. 4, pp. 676-697, 200, doi: https://doi.org/10.1002/nme.1782.

[8] M. Eslami and A. Bahtui, *Coupled Thermoelasticity of Thin Cylindrical Shells Made of Functionally Graded Material*. Na, 2005.

[9] Eslami, M.R., Shakeri, M., and Shiari, B., "Coupled Thermoelasticity of Composite Laminated Cylindrical Shells", Proc. ASME-ESDA, Montpellier, France, 1996.

[10] B. Shiari, "Thermomechanical Shocks in Composite Cylindrical Shells: A Coupled Thermoelastic Finite Element Analysis," *Scientia Iranica*, Vol. 10, No. 1, pp. -, 2003. [Online]. Available: https://scientiairanica.sharif.edu/article_2663_78aa19f83998fdf8a879c8b0812e7321.pdf.

[11] M. Jafarinezhad and M. Eslami, "Coupled Thermoelasticity of FGM Annular Plate under Lateral Thermal Shock," *Composite Structures*, Vol. 168, pp. 758-771, 2017, doi: https://doi.org/10.1016/j.compstruct.2017.02.071.

[12] N. Wu, B. Rauch, and P. Kessel, "Perturbation Solutiontothe Dynamic Responseof OrthotropicCylindricalL Shellsusingthe Generalized TheoryofThermoelasticity," *Journal of Thermal Stresses*, Vol. 14, No. 4, pp. 465-477, 1991, doi: https://doi.org/10.1080/01495739108927080.

[13] H. Eliasi, M. Bateni, and M. Eslami, "Coupled Thermoelasticity of FGM Truncated Conical Shells," *Iranian Journal of Mechanical Engineering Transactions of the ISME*, Vol. 22, No. 1, pp. 127-142, 2021, doi: https://doi.org/10.30506/jmee.2021.131971.1239.

[14] A. Baghlani, M. Khayat, and S. M. Dehghan, "Free Vibration Analysis of FGM Cylindrical Shells Surrounded by Pasternak Elastic Foundation in Thermal Environment

Considering Fluid-structure Interaction," *Applied Mathematical Modelling,* Vol. 78, pp. 550-575, 2020, doi: https://doi.org/10.1016/j.apm.2019.10.023.

[15] A. Alibeigloo, "Coupled ThermoelasticityAnalysis of Carbon Nano Tube Reinforced Composite Rectangular Plate Subjected to Thermal Shock," *Composites Part B: Engineering,* Vol. 153, pp. 445-455, 2018,doi: https://doi.org/10.1016/j.compositesb.2018.09.003.

[16] A. Akbarzadeh, M. Abbasi, and M. Eslami, "Coupled Thermoelasticity of Functionally Graded Plates Based on the Third-order Shear Deformation Theory," *Thin-Walled Structures,* Vol. 53, pp. 141-155, 2012, doi: https://doi.org/10.1016/j.tws.2012.01.009.

[17] Y. Heydarpour and M. Aghdam, "Transient Analysis of Rotating Functionally Graded Truncated Conical Shells Based on the Lord–Shulman Model," *Thin-Walled Structures,* Vol. 104, pp. 168-184, 2016, doi: https://doi.org/10.1016/j.tws.2016.03.016.

[18] E. McQuillen and M. Brull, "Dynamic ThermoelasticResponse of Cylindrical Shells," Journal of applied Mechanics, Vol. 37(3), pp. 661-670, 1970, doi: https://doi.org/10.1115/1.3408595.

[19] Eslami, M.R., Lecture on "Coupled Thermoelasticity of Plates and Shells", Polish Academy of Sciences, (IPPT-PAN), Warsaw, June 22, 1998.

[20] Eslami, M.R., Lecture on "A New Approach to the Numerical Solutions of Coupled Thermoelasticity", Polish Academy of Sciences, (IPPT-PAN), Warsaw, June 26, 1998.

[21] J. Reddy, "An Introduction to Nonlinear Finite Element Analysis," 2004, Oxford University Press, https://doi.org/10.1093/acprof:oso/9780198525295.001.0001.

[22] M. R. Eslami, *Finite Elements Methods in Mechanics*, Switzerland Springer, 2014, https://doi.org/10.1007/978-3-319-08037-6.

[23] M. R. Eslami, *Finite Elements Methods in Mechanics*, Switzerland Springer, 2014, https://doi.org/10.1007/978-3-319-08037-6.

[24] S. Y. Chang, "Studies of Newmark Method for Solving Nonlinear Systems:(I) Basic Analysis," *Journal of the Chinese Institute of Engineers*, Vol. 27, No. 5, pp. 651-662, 2004, doi: https://doi.org/10.1080/02533839.2004.9670913.

[25] S. Y. Chang, "Studies of Newmark Method for Solving Nonlinear Systems:(II) Verification and Guideline," *Journal of the Chinese Institute of Engineers,* Vol. 27, No. 5, pp. 663-675, 2004, doi: https://doi.org/10.1080/02533839.2004.9670914.

[26] J. Duan and Y.-G. Li, "Solving the Kinetic Equations with Geometric Nonlinearity Considered," in *2017 3rd International Forum on Energy, Environment Science and Materials (IFEESM 2017)*, 2018: Atlantis Press, pp. 234-238, doi: https://doi.org/10.2991/ifeesm-17.2018.44.

[27] H. Eliasi, G. H. Payganeh, M. Shahgholi, and M. R. Eslami, "Stability of Thin Cylindrical Shells under Coupled ThermoelasticAssumption," *Journal of Thermal Stresses*, Vol. 46, No. 10, pp. 1003-1021, 2023, doi: https://doi.org/10.1080/01495739.2023.2216743.

[28] G. Sheng, X. Wang, G. Fu, and H. Hu, "The Nonlinear Vibrations of Functionally Graded Cylindrical Shells Surrounded by an Elastic Foundation," *Nonlinear Dynamics*, Vol. 78, pp. 1421-1434, 2014, doi: https://doi.org/10.1007/s11071-014-1525-8.

Appendix

$$A_{11} = A_{22} = \int E(z)dz$$
$$A_{12} = \int E \vdash (z)\upsilon dz$$
$$A_{55} = \frac{\int E(z)}{2(1+\upsilon)dz}$$
$$B_{11} = B_{22} = \int E(z)zdz$$
$$B_{12} = \int E(z)z\upsilon dz$$
$$D_{11} = D_{\{22\}} = \int E(z)z^{2dz}$$
$$D_{12} = \int E(z)z^{2\upsilon dz}$$
$$R_1 = \int E(z)\alpha(z)dz$$
$$R_{12} = \int E(z)\alpha(z)\upsilon dz$$
$$R_2 = \int E(z)\alpha(z)zdz$$
$$R_{22} = \int E(z)\alpha(z)z\upsilon dz$$
$$R_3 = \int E(z)\alpha(z)z^{2dz}$$
$$R_{32} = \int E(z)\alpha(z)z^{2\upsilon dz}$$
$$C_{11} = \int \rho(z)c(z)dz$$
$$C_{22} = \int \rho(z)c(z)zdz$$
$$C_{33} = \int \rho(z)c(z)z^{2dz}$$
$$K_1 = \int K(z)dz$$
$$K_2 = \int K(z)zdz$$
$$K_3 = \int K(\mathrm{z})z^2dz$$